ACS APPLIED MATERIALS & INTERFACES

Research Article

www.acsami.org

Unique Device Operations by Combining Optical-Memory Effect and Electrical-Gate Modulation in a Photochromism-Based Dual-Gate Transistor

Yasushi Ishiguro,[†,‡] Ryoma Hayakawa,[‡] Takeshi Yasuda,[§] Toyohiro Chikyow,[‡] and Yutaka Wakayama*[,†,‡]

[†]Department of Chemistry and Biochemistry, Faculty of Engineering, Kyushu University, 1-1 Namiki, Tsukuba, Ibaraki 305-0044, Japan

[‡]International Center for Materials Nanoarchitectonics (WPI-MANA), National Institute for Materials Science (NIMS), 1-1 Namiki, Tsukuba, Ibaraki 305-0044, Japan

[§]Photovoltaic Materials Unit, National Institute for Materials Science (NIMS), 1-2-1 Sengen, Tsukuba, Ibaraki 305-0047, Japan

Supporting Information

ABSTRACT: We demonstrate a new device that combines a light-field effect and an electrical-gate effect to control the drain current in a dual-gate transistor. We used two organic layers, photochromic spiropyran (SP)-doped poly(triarylamine) (PTAA) and pristine PTAA, as top and bottom channels, respectively, connected to common source and drain electrodes. The application of voltage to the top and bottom gates modulated the drain current through each layer independently. UV irradiation suppressed the drain current through the top channel. The suppressed current was then maintained even after the UV light was turned off because of an optical memory effect induced by photoisomerization of SP. In contrast, UV irradiation did not change the drain current in the bottom channel. Our dual-gate transistor thus has two organic channels with distinct photosensitivities: an optically active SP-PTAA film and an optically inactive PTAA film. This device configuration allows multi-level switching via top- and bottom-gate electrical fields with an optical-memory effect.

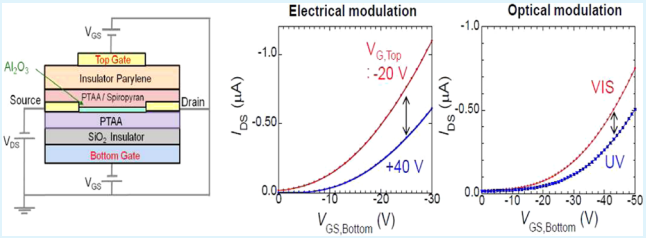

KEYWORDS: *organic transistor, photochromism, dual-gate transistor, optical-memory effect, spiropyran, poly(triarylamine)*

1. INTRODUCTION

Organic field-effect transistors (OFETs) have been extensively studied over the last several years. Great progress has been made in improving their performance. High carrier mobilities of up to 10 $cm^2/(V\ s)$ have been achieved in solution-processed organic semiconductors.[1−3] The further evolution of organic devices demands the integration of specific functionalities into conventional OFETs.

To this end, optically controllable OFETs based on photochromic molecules have been proposed. Photochromic molecules such as diarylethene and azobenzene are used as photosensitive components at the interface between organic semiconductors and gate insulator layers,[4,5] inside polymeric semiconductors or polymeric gate insulators,[6−13] in the side chains of polymeric semiconductors,[14,15] or in direct channel layers.[16] The drain current can be reversibly controlled in accordance with the photoisomerization. We previously achieved optical switching of transistor properties by adopting photoisomerized spiropyran (SP) molecules dispersed in a poly(triarylamine) (PTAA) single channel layer.[17] The drain current (I_{DS}) was reduced by ultraviolet UV irradiation and restored by visible (VIS) light irradiation. The ionic-polarized open-ring SP isomer worked as a carrier scattering site to suppress the carrier transport effectively in the polymer channel.

Dual-gate OFETs are promising high-performance candidates. The device configuration makes it possible to induce a large drain current under dual gate bias voltages, leading to great improvement of carrier mobility.[18−20] In addition, the threshold voltage can be controlled by a combination of double gates.[21−26] Several devices based on these features, including pH sensors and chemical sensors, have been proposed.[27,28] Kippelen et al. proposed a dual-gate transistor made of 6,13-bis(triisopropylsilylethynyl) pentacene (TIPS-pentacene) and PTAA heterolayers. The TIPS-pentacene and PTAA films work as top and bottom channels, respectively. The top channel showed high carrier mobility of up to 16×10^{-2} $cm^2/(V\ s)$, and the bottom channel showed low carrier mobility of 3.8×10^{-2} $cm^2/(V\ s)$.[29] The respective transistor channels are switched by the top and bottom gates. We ascribe the advantage of the dual-gate transistors to the capability to combine different operations in the top and bottom channels, which would

Received: July 16, 2013
Accepted: September 16, 2013
Published: September 16, 2013

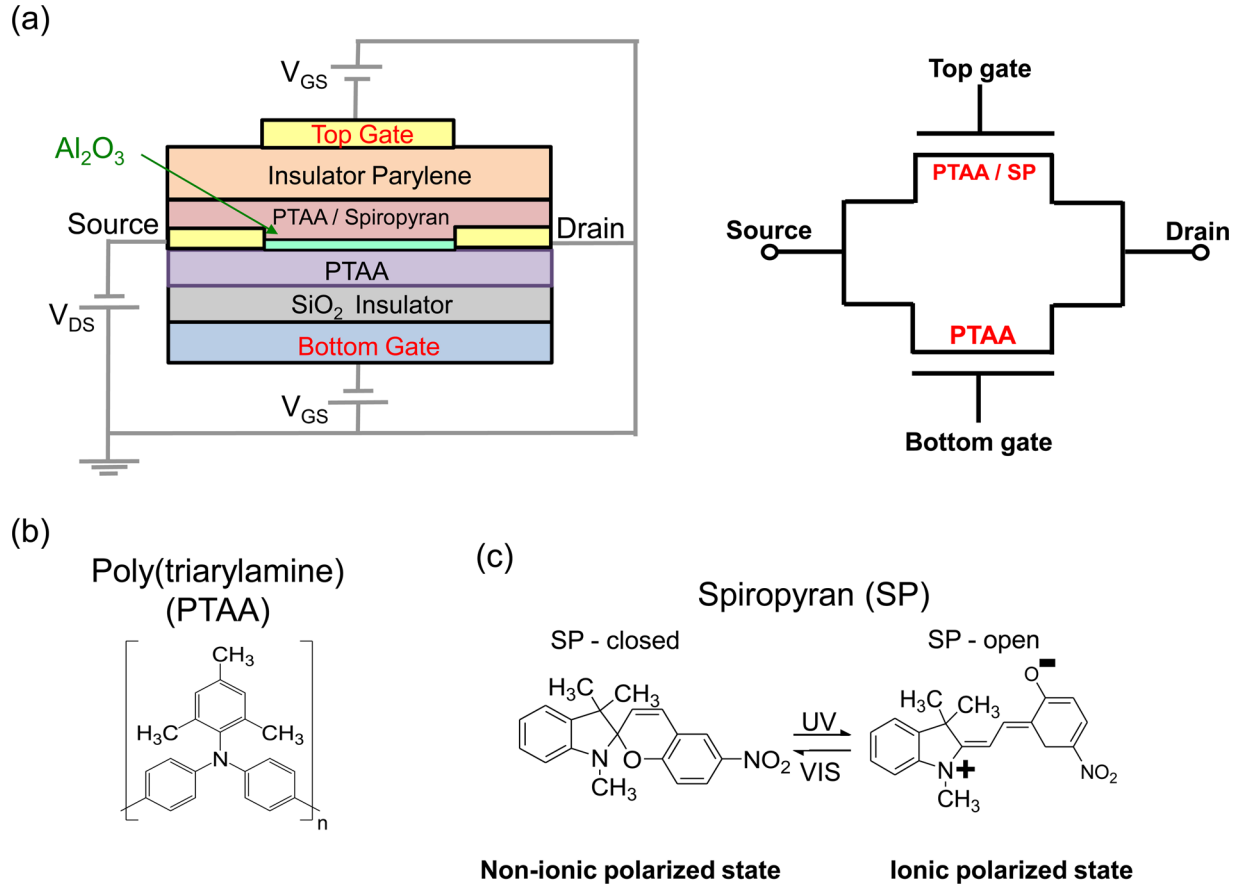

Figure 1. (a) Device configuration and circuit diagram of photochromism-based dual-gate transistor. (b) Chemical structure of PTAA. (c) Conformation change of SP molecules between ionic-polarized open ring and nonionic closed ring. The photoisomerization is reversibly controlled by the alternation of UV and VIS light.

allow the integration of new functionalities into conventional organic transistors.

In this study, we integrated a light-field effect into a conventional dual-gate OFET. In the photochromism-based dual-gate OFET, the transistor channels consist of an SP-doped PTAA film and a pristine PTAA film (Figure 1). An aluminum oxide (Al_2O_3) thin film is inserted between the organic layers to prevent diffusion of SP molecules from the upper layer to the lower layer. The top and bottom layers work as transistor channels independently. Importantly, optical switching of the drain current is achievable only in the top layer, owing to photoisomerization of SP between a nonionic closed ring and an ionic-polarized open-ring. Tuning of gate bias voltages can adjust such optical responsivity in the transistor.

2. EXPERIMENTAL SECTION

Highly doped *p*-type Si wafers with a 200 nm-thick SiO_2 layer were used as substrates for the fabrication of dual gate-OFETs. The Si substrate works as a bottom-gate electrode and the SiO_2 layer as an insulator. PTAA molecules were dissolved in toluene at a concentration of 1 wt %. The PTAA films were formed by spin-coating (1000 rpm, 1 min) on substrate pretreated with hexamethyldisilazane to improve wettability and to reduce charge trapping sites at the interface between the SiO_2 and PTAA layers. The samples were then heat-annealed at 100 °C for 1 h to remove residual solvents. The thickness of the PTAA film was estimated to be 100 ± 10 nm by surface profilometer (Dektak 6M). Subsequently, interdigitated Au electrodes were deposited as source and drain electrodes on top of the PTAA film through a metal shadow mask. The channel length and width of the transistors were 75 μm and 5 mm, respectively. To prevent the diffusion of SP molecules from the upper SP-PTAA layer to the lower PTAA layer, a 2.2 nm-thick Al_2O_3 layer was grown on the PTAA film by atomic layer deposition at a substrate temperature of 120 °C. The electrical contact to the upper SP-PTAA layer was not affected by the Al_2O_3 layer because the Al_2O_3 film was deposited favorably only on the PTAA layer and no film was formed on the electrodes due to the inertness of the Au surface. A mixture of PTAA and SP (1:1 weight ratio) dissolved in toluene at 1 wt % was spin-coated (1000 rpm, 1 min) on the Al_2O_3 layer to form the SP-PTAA film. On top of the SP-PTAA film, Parylene-C was deposited by chemical vapor deposition as the top gate insulator. The thickness of the films was estimated to be 1.3 μm by the Dektak 6M. Finally, as the top-gate electrode, a 20 nm-thick Au electrode was deposited on the SP-PTAA film through a metal shadow mask.

The electrical characteristics of the transistors were measured with a semiconductor device analyzer (Agilent B1500A) in a vacuum chamber (10^{-1} Pa) at room temperature. A xenon lamp was used as the light source for the photoisomerization of the SP. Band-pass filters passed UV light at 340 nm (0.14 mW/cm^2 by power meter) to generate an ionic polarized open-ring isomer and VIS light at 550 nm (1.13 mW/cm^2) to transform the open-ring isomer into a closed-ring isomer. The irradiation time was fixed at 10 min, which is enough to induce optical switching of the drain current. This is based on our preliminary experiment to examine the time dependence of the drain current upon UV and VIS light irradiation (Figure S1, Supporting Information).

3. RESULTS AND DISCUSSION

3.1. Transistor Properties in Top and Bottom Channels in a Dual-Gate Transistor. When the top gate

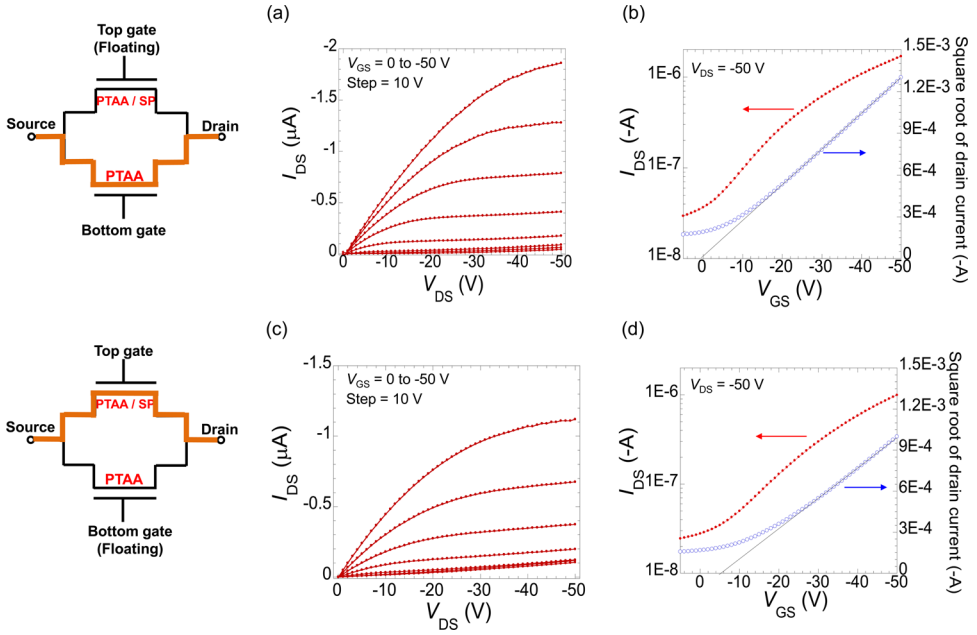

Figure 2. (a) Output and (b) transfer characteristics in the bottom channel when the top gate is electrically floated. (c) Output and (d) transfer characteristics in the top channel when the bottom gate is electrically floated. The SP dispersed in the PTAA is in the closed-ring state. This state had no influence on carrier transport in the top channel.

was electrically floated, the current flowed through the bottom (PTAA) channel (Figure 2 top left, orange line), and the drain current (I_{DS}) in the output curve increased linearly at a low drain voltage (Figure 2a), proving a low contact resistance between the electrodes and channel layers. The carrier mobility (μ) and the threshold voltage (V_{th}) estimated from saturation regime in the transfer curve (Figure 2b) were $\mu = 2.3 \times 10^{-4}$ cm^2/(V s) and $V_{th} = 0.7$ V. These values are comparable to those in a pristine PTAA transistor.[17] When the bottom gate was electrically floated, the current flowed through the top (SP-PTAA) channel (Figure 2 bottom left, orange line). The estimated carrier mobility and threshold voltage of the top channel were $\mu = 1.8 \times 10^{-4}$ cm^2/(V s) and $V_{th} = -3.9$ V. Thus, the SP-PTAA layer was confirmed to work as the top transistor channel and the pristine PTAA layer as the bottom transistor channel.

The difference of transistor properties between top and bottom channels is probably caused by variation in the interface roughness between gate insulator and organic semiconductor layers because the interface roughness between the Parylene-C and SP-PTAA layers was higher than that between the SiO_2 and PTAA layers (Figure S2, Supporting Information). The nonionic closed-ring SPs in the top channel layer may have an affect on the carrier mobility because the molecules have dipole moment (>6 D).[6] However, we had already confirmed that the closed-ring SP molecules had no influence on the transistor properties because the transistor properties of the closed-ring SP/PTAA blend were almost comparable to those of a pristine PTAA transistor.[17] Therefore, we concluded that the differences in the transistor properties can be attributed to the interface roughness.

3.2. Impact of Light Irradiation on Carrier Transport through Top and Bottom Channels. As the two organic channels have distinct photosensitivities, different photo-responsivities can be induced in the top and bottom channels. The drain current through the PTAA bottom channel was not changed by the alternation of UV and VIS irradiation (Figures 3a, S3a, and S3b, Supporting Information). Thus, the bottom transistor channel is inactive upon irradiation.[17,30,31] In

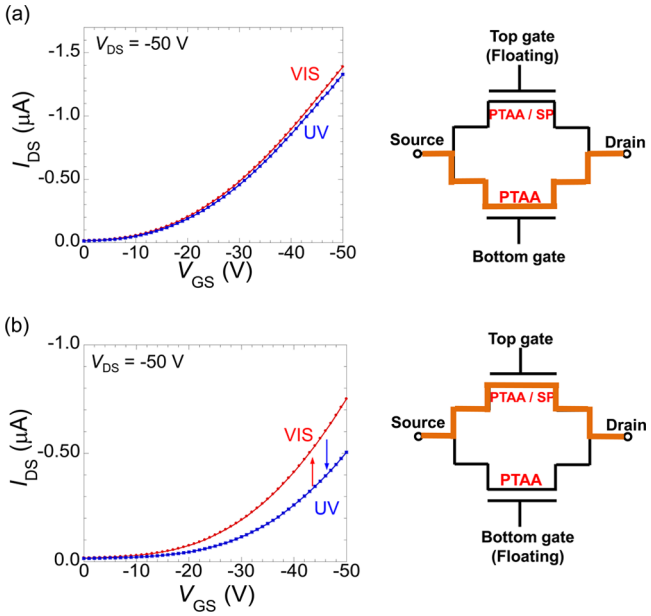

Figure 3. (a) Change in transfer characteristics of bottom channel at V_{DS} of −50 V under UV or VIS irradiation for 30 min. (b) Reversible change in transfer characteristics of the top channel at V_{DS} of −50 V by alternating UV and VIS irradiation.

contrast, the drain current through the SP-PTAA top channel was reduced by UV irradiation. The reduction rate was estimated to be about 6 % when the concentration of SP-open was doubled upon UV irradiation. The reduced drain current was restored by subsequent VIS irradiation (Figures 3b, S3c, and S3d, Supporting Information). The photo-switching behavior is consistent with our previous report:[17] the open-ring SP has an ionic polarized structure, which works as a carrier

dx.doi.org/10.1021/am402833k | ACS Appl. Mater. Interfaces 2013, 5, 9726−9731

scattering site in the PTAA channel layer to suppress the carrier transport. Meanwhile, we confirmed that the transistor properties of the closed-ring SP/PTAA blend were almost comparable to those of a pristine PTAA transistor; i.e., the closed-ring SP molecules have no influence on the transistor properties.[17]

To compare the obtained results with a top contact geometry for the optically controllable layer, we fabricated the opposite device architecture by putting the SP-PTAA layer under the Al_2O_3 layer and the PTTA on the top of it. The drain current through the SP-PTAA bottom channel was confirmed to be reduced by UV irradiation and restored by VIS irradiation. In contrast, the drain current through the PTAA top channel was not changed by the alternation of UV and VIS light irradiation (Figure S4, Supporting Information). These results demonstrate potential of various device architectures. However, the reduction rate was smaller than that of the opposite architecture (Figure 3b) due to light absorption by the upper PTAA layer. In conclusion, the photoactive SP/PTAA layer should be the upper channel to obtain higher photosensitivity because of effective light irradiation.

Importantly, the light-induced variation in I_{DS} was maintained even after the irradiation was turned off, in contrast to the electrical-gate modulation of I_{DS} described in Figure 2. These results indicate that the SP-doped top channel shows an optical-memory effect. Thus, our dual-gate transistor allows two distinct device operations upon irradiation: optically controllable and nonresponsive operations through the top and bottom channels.

The SP molecule undergoes the thermal transformation from the open-ring SP to the closed-ring SP. However, we confirmed that the applied electronic field has no effect on the thermal transformation of SP molecule in our previous work.[17] The photo-switching behavior was repeated up to several cycles (Figure S5, Supporting Information). It should be noted that the drain current gradually decreased with repeated optical switching. The degradation in the switching property can be ascribed to the deterioration of SP molecules upon light irradiation.[17]

3.3. Electrical Modulation of Drain Current by Dual Gates. The drain current of the dual-gate transistor can be controlled by both top and bottom gates. This section describes a dual-gate modulation of the drain current controlled by the dual electrical-field effect.

As the top gate voltage increased from −40 to +40 V, the drain current, plotted as a function of bottom gate voltage, was gradually reduced (Figure 4a). The threshold voltage (V_{th}) determined from the $I_{DS}^{1/2}$ vs. V_{GS} plots (Figure S6, Supporting Information) shifted from +4 to −4 V when the top gate voltage increased from −40 to +40 V (Figure 4b). These results indicate that the application of a positive top-gate voltage formed a depletion layer in the bottom channel. Thus, more-negative voltage in the bottom gate was required to compensate for the depletion layer and to form the transistor channel. As a consequence, an increasing top-gate voltage made the threshold voltage of the bottom channel more negative.

Generally, the shift in V_{th} as a function of top gate bias can be given by $V_{th} = (-C_{Top}/C_{Bottom})\cdot V_{G,Top}$,[16] where C_{Top} and C_{Bottom} are unit-area capacitances in each dielectric layer. C_{Top} of Parylene-C was 2.4 nF/cm^2 and C_{Bottom} of SiO_2 was 18.5 nF/cm^2. Thus, C_{Top}/C_{Bottom} = 0.13. The value of C_{Top}/C_{Bottom} estimated from the slope of the curve in Figure 4b was 0.10, which agrees well, indicating that the threshold voltage in this

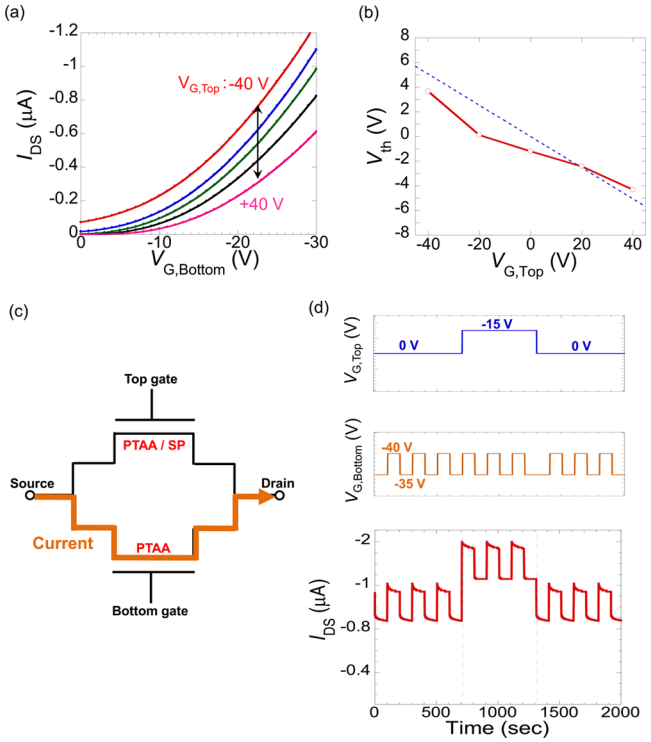

Figure 4. (a) Change in the drain current as a function of the bottom gate voltage. Additional top gate voltage was supplied from −40 to +40 V in steps of 20 V. (b) Red line: change in the threshold voltage (V_{th}) against top-gate voltage. Dashed line: theoretical slope when capacitance of Parylene-C (2.7 nF/cm^2) is divided by that of SiO_2 (18.5 nF/cm^2). (c) Circuit diagram of the transistor with current path depicted by an orange line. (d) Electrical modulation of the drain current by top and bottom gates. The drain current through the top channel was modulated by top and bottom gates. The output signal (I_{DS}) was monitored as functions of $V_{G,Top}$ and $V_{G,Bottom}$ input signals.

dual-gate transistor was electrically controllable in the same way as in conventional dual-gate transistors.[21−26]

We examined dual-gate modulation of the drain current on the basis of our finding that the threshold voltage can be controlled by the top and bottom gates. The top channel was used for the current path (Figure 4c). The top and bottom gate voltages were supplied separately as input signals (Figure 4d, top and middle). The resulting I_{DS} was obtained as an output signal (Figure 4d, bottom). From 0 to 700 s, while the bottom gate was grounded, I_{DS} was modulated between ca. −0.9 and −1.2 μA according to the input signal from the top gate, where the gate voltage ($V_{G,Top}$) was varied between −35 and −40 V. From 700 to 1300 s, $V_{G,Bottom}$ of −15 V was applied, raising the modulation I_{DS} to between ca. −1.3 and −1.6 μA. When $V_{G,Bottom}$ was set to 0 V again, I_{DS} was restored to its initial range. These results clearly show that the drain current can be electrically modulated by two input signals from dual gates.

3.4. Dual-Gate Switching of Light-Field Effect in Transistor Properties. On the basis of the results in sections 3.2 and 3.3, we manipulated optical responsively in the dual-gate transistor by fine tuning the top and bottom gate voltages to control the current path. Combining the light-field effect and electrical-gate modulation enabled multi-level switching of the drain current with an optical-memory effect by three input signals: top and bottom gates and light irradiation. $V_{G,Top}$ and UV light acted as input signals. $V_{G,Bottom}$ selected the transistor channel: top, bottom, or both.

When the bottom gate was grounded, current flowed only through the top channel: it was selected as the transistor channel (Figure 5a). First, $V_{G,Top}$ was varied between −35 and −40 V every 100 to 600 s. In response, I_{DS} varied between −0.32 and −0.22 μA. Following UV irradiation for 10 min, I_{DS} was lowered and varied between −0.22 and −0.13 μA. The modulation width (0.09−0.10 μA) was almost constant even after irradiation: that is, an optical memory effect was induced by the photoisomerization of SP from a nonionic state to an ionic polarized state. When a $V_{G,Bottom}$ of −20 V was applied, part of the I_{DS} passed through the optically inactive bottom channel, so the optically induced variation in I_{DS} was decreased (Figure 5b). When $V_{G,Bottom}$ was increased to −30 V, current flowed only through the bottom channel, so there was no change in I_{DS} even after irradiation (Figure 5c). These results clearly show that the photoresponsivity of the transistor can be chosen by optimization of the top and bottom gate voltages.

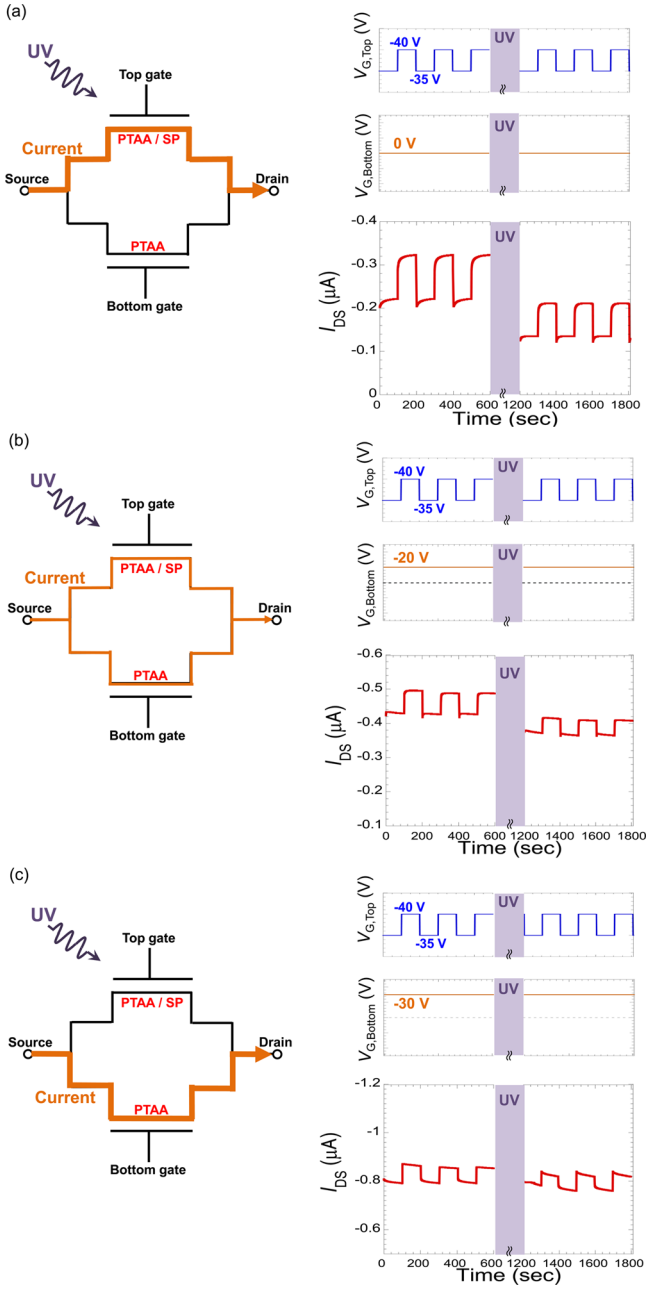

Figure 5. Optical and electrical modulation of drain current. Input signals were top-gate voltage (−35 to −40 V) and UV light (10 min). (a) The bottom-gate was grounded, and current flowed only in the top channel. (b) A bottom-gate voltage of −20 V divided the drain current between channels. (c) At a bottom-gate voltage of −30 V, current flowed only in the bottom channel. UV irradiation caused no variation in drain current, although the current was modulated by the top-gate voltage.

To test the unique combination of the optical and electrical modulation of drain current, we varied $V_{G,Top}$ between −35 and −40 V every 100 s, used $V_{G,Bottom}$ to switch current paths between the top ($V_{G,Bottom}$ = 0 V) and bottom channels (−30 V), and periodically applied UV light (Figure 6). From 0 to 600 s, I_{DS} through the bottom channel was modulated between −0.1 and −0.2 μA according to the input signal from the top gate. From 600 to 2200 s, the application of $V_{G,Bottom}$ = −30 V raised I_{DS} to between −0.8 and −0.9 μA. During this period, UV irradiation had no effect on I_{DS}, which was flowing through the nonphotoactive bottom channel. From 2200 to 4000 s, the application of $V_{G,Bottom}$ = −10 V lowered I_{DS} by changing the dominant current path from the bottom channel to the photoactive top channel. UV irradiation caused photoisomerization of SP, furthering lowering I_{DS}. From 4000 s, the bottom gate voltage was returned to −30 V, making the bottom channel again dominant. I_{DS} did not change with UV irradiation, and the optical memory function disappeared. These results show the unique combination of the optical memory effect and electrical-gate modulation in the dual-gate transistor.

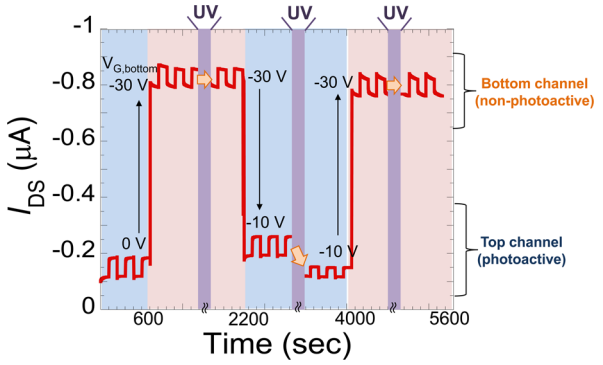

Figure 6. Manipulation of drain current by a combination of optical and electrical gates. The drain current was controlled by the top and bottom gates and by UV irradiation.

4. CONCLUSIONS

By integrating an optical memory effect into a conventional dual-gate OFET, we have developed a new type of dual-gate transistor. The combination of an optically active SP-PTAA film (as the top channel) and an optically inactive PTAA film (as the bottom channel) creates a dual-gate transistor with two distinct operations upon light irradiation. The optically induced change in the drain current was maintained after UV irradiation was turned off, indicating that the SP-doped top channel behaves as an optical memory. Optimizing the dual gate voltages to control the current path allows the optical responsivity to be chosen. These features make it possible to manipulate the drain current by three parameters: the top and bottom gates and irradiation. Our findings will enable the development of new device applications such as optically and

electrically controllable electric circuits and lead to the integration of new functionalities into conventional organic transistors.

■ ASSOCIATED CONTENT

Supporting Information

Additional results, including AFM images of top and bottom channel interfaces, detailed output and transfer characteristics for the dual-gate transistor operation, and time dependence of the optical modulation. This material is available free of charge via the Internet at http://pubs.acs.org.

■ AUTHOR INFORMATION

Corresponding Author

*E-mail: wakayama.yutaka@nims.go.jp.

Notes

The authors declare no competing financial interest.

■ REFERENCES

(1) Nakayama, K.; Hirose, Y.; Soeda, J.; Yoshizumi, M.; Uemura, T.; Uno, M.; Li, W.; Kang, M. J.; Yamagishi, M.; Okada, Y.; Miyazaki, E.; Nakazawa, Y.; Nakao, A.; Takimiya, K.; Takeya, J. *Adv. Mater.* **2011**, *23*, 3309−3314.

(2) Ou-Yang, W.; Uemura, T.; Miyake, K.; Onishi, S.; Kato, T.; Katayama, M.; Kang, M. J.; Takimiya, K.; Ikeda, M.; Kuwabara, H.; Hamada, M.; Takeya, J. *Appl. Phys. Lett.* **2012**, *101*, 223304−223308.

(3) Minemawari, H.; Yamada, T.; Matsui, H.; Tsutsumi, J.; Haas, S.; Chiba, R.; Kumai, R.; Hasegawa, T. *Nature* **2011**, *475*, 364−367.

(4) Yoshida, M.; Suemori, K.; Uemura, S.; Hoshino, S.; Takada, N.; Kodzasa, T.; Kamata, T. *Jpn. J. Appl. Phys.* **2010**, *49*, 04DK09-1−04DK09-4.

(5) Zhang, H.; Guo, X.; Hui, J.; Hu, S.; Xu, W.; Zhu, D. *Nano Lett.* **2011**, *11*, 4939−4946.

(6) Li, Y.; Zhang, H.; Qi, C.; Guo, X. *J. Mater. Chem.* **2012**, *22*, 4261−4265.

(7) Orgiu, E.; Crivillers, N.; Herder, M.; Grubert, L.; Pätzel, M.; Frisch, J.; Pavlica, E.; Duong, D. T.; Bratina, G.; Salleo, A.; Koch, N.; Hecht, S.; Samorì, P. *Nat. Chem.* **2012**, *4*, 675−679.

(8) Lutsyk, P.; Janus, K.; Janus, Sworakowski, J.; Generali, G.; Capelli, R.; Muccini, M. *J. Phys. Chem. C* **2011**, *115*, 3106−3114.

(9) Lutsyk, P.; Janus, K.; Sworakowski, J.; Kochalska, A.; Nešpůrek, S. *Chem. Phys.* **2012**, *404*, 22−27.

(10) Kratochvílová, I.; Nešpůrek, S.; Šebera, J.; Záliš, S.; Pavelka, M.; Wang, G.; Sworakowski, J. *Eur. Phys. J. E* **2008**, *25*, 299−307.

(11) Shen, Q.; Cao, Y.; Liu, S.; Steigerwald, M. J.; Guo, X. *J. Phys. Chem. C* **2009**, *113*, 10807−10812.

(12) Shen, Q.; Wang, L.; Liu, S.; Cao, Y.; Gan, L.; Guo, X.; Steigerwald, M. J.; Shuai, Z.; Liu, Z.; Nuckolls, C. *Adv. Mater.* **2010**, *22*, 3282−3287.

(13) Crivillers, N.; Orgiu, E.; Reinders, F.; Mayor, M.; Samorì, P. *Adv. Mater.* **2011**, *23*, 1447−1452.

(14) Guo, X.; Huang, L.; O'Brien, S.; Kim, P.; Nuckolls, C. *J. Am. Chem. Soc.* **2005**, *127*, 15045−15047.

(15) Bardavid, Y.; Goykhman, I.; Nozaki, D.; Cuniberti, G.; Yitzchaik, S. *J. Phys. Chem. C* **2011**, *115*, 3123−3128.

(16) Hayakawa, R.; Higashiguchi, K.; Matsuda, K.; Chikyow, T.; Wakayama, Y. *ACS Appl. Mater. Interfaces* **2013**, *5*, 3625−3630.

(17) Ishiguro, Y.; Hayakawa, R.; Chikyow, T.; Wakayama, Y. *J. Mater. Chem. C* **2013**, *1*, 3012−3016.

(18) Maddalena, F.; Spijkman, M.; Brondijk, J.; Fontejin, P.; Brouwer, F.; Hummelen, J. C.; Leeuw, D. M.; Blom, P. W.; Boer, B. *Org. Electron.* **2009**, *9*, 839−846.

(19) Yamagishi, M.; Takeya, J.; Tominari, Y.; Nakazawa, Y.; Kuroda, T.; Ikehata, S.; Uno, M.; Nishikawa, T.; Kawase, T. *Appl. Phys. Lett.* **2007**, *90*, 182117−182119.

(20) Morana, M.; Bret, G.; Brabec, C. *Appl. Phys. Lett.* **2005**, *87*, 153511−153513.

(21) Spijkman, M.-J.; Myny, K.; Smits, E. C. P.; Heremans, P.; Blom, P. W. M.; deLeeuw, D. M. *Adv. Mater.* **2011**, *23*, 3231−3242.

(22) Iba, S.; Sekitani, T.; Kato, Y.; Someya, T.; Kawaguchi, H.; Takamiya, M.; Sakurai, T.; Takagi, S. *Appl. Phys. Lett.* **2005**, *87*, 023509−023511.

(23) Gelinck, G. H.; van Veenendaal, E.; Coehoorn, R. *Appl. Phys. Lett.* **2005**, *87*, 073508−073510.

(24) Koo, J. B.; Ku, C. H.; Lim, J. W.; Kim, S. H. *Org. Electron.* **2007**, *8*, 552−558.

(25) Tsamados, D.; Cvetkovic, N. V.; Sidler, K.; Bhandari, J.; Savu, V.; Brugger, J.; Ionescu, A. M. *Solid-State Electron.* **2010**, *54*, 1003−1009.

(26) Spijkman, M.; Smits, E. C. P.; Blom, P. W. M.; de Leeuw, D. M.; Bon Saint Côme, Y.; Setayesh, S.; Cantatore, E. *Appl. Phys. Lett.* **2008**, *92*, 143304−143306.

(27) Park, Y. M.; Salleo, A. *Appl. Phys. Lett.* **2009**, *95*, 133307−133309.

(28) Spijkman, M.-J.; Brondijk, J. J.; Geuns, T. C. T.; Smits, E. C. P.; Cramer, T.; Zerbetto, F.; Stoliar, P.; Biscarini, F.; Blom, P. W. M.; de Leeuw, D. M. *Adv. Funct. Mater.* **2010**, *20*, 898−905.

(29) Hwang, D. K.; Fuentes-Hernandez, C.; Berrigan, J. D.; Fang, Y.; Kim, J.; Potscavage, W. J., Jr.; Cheun, H.; Sandhage, K. H.; Kippelen, B. *J. Mater. Chem.* **2012**, *22*, 5531−5537.

(30) Newman, C. R.; Sirringhaus, H.; Blakesley, J. C.; Speller, R. *Appl. Phys. Lett.* **2007**, *91*, 142105−142107.

(31) Intaniwet, A.; Mills, C. A.; Shkunov, M.; Thiem, H.; Keddie, J. L.; Sellin, P. J. *J. Appl. Phys.* **2009**, *106*, 064513−062518.